Neuropathological correlates and genetic architecture of microglial activation in elderly human brain

Daniel Felsky PhD[1,2,*], Tina Roostaei MD[1], Kwangsik Nho PhD[3], Shannon L. Risacher PhD[3], Elizabeth M. Bradshaw PhD[1], Vlad Petyuk PhD[4], Julie A Schneider MD[5,6], Andrew Saykin MD[3], David A. Bennett MD[5,6], Philip L. De Jager MD[1,2]

1. Center for Translational and Computational Neuroimmunology, Department of Neurology, Columbia University Medical Center, 630 West 168th Street, New York, NY 10032, USA.
2. Program in Population and Medical Genetics, Broad Institute of MIT and Harvard, 320 Charles Street, Cambridge, MA 02141, USA.
3. Indiana Alzheimer's Disease Center, Center for Neuroimaging, Department of Radiology and Imaging Sciences, Center for Computational Biology and Bioinformatics, Indiana University School of Medicine, 355 West 16th Street, Indianapolis, IN 46202, USA.
4. Pacific Northwest National Laboratory, Richland, WA, 99354, USA
5. Department of Neurology, Rush University Medical Center, 1653 West Congress Parkway, Chicago, IL 60612, USA.
6. Rush Alzheimer's Disease Center, Rush University Medical Center, 1653 West Congress Parkway, Chicago, IL 60612, USA.

[*]Corresponding author: Daniel Felsky
Center for Translational and Computational Neuroimmunology (CTCN)
Columbia University Medical Center
630 West 168th St., PH 19 – 302
New York, NY 10032
Tel: (781)-686-7215
Email, institutional: df2652@columbia.edu
Email, alternate: dfelsky@gmail.com

Abstract

Microglia, the resident immune cells of the brain, have important roles in brain health. However, little is known about the regulation and consequences of microglial activation in the aging human brain. We assessed the effect of microglial activation in the aging human brain by calculating the proportion of activated microglia (PAM), based on morphologically defined stages of activation in four regions sampled postmortem from up to 225 elderly individuals. We found that cortical and not subcortical PAM measures were strongly associated with β-amyloid, tau-related neuropathology, and rates of cognitive decline. Effect sizes for PAM measures are substantial, comparable to that of *APOE* ε4, the strongest genetic risk factor for Alzheimer's disease. Mediation modeling suggests that PAM accelerates accumulation of tau pathology leading to cognitive decline, supporting an upstream role for microglial activation in Alzheimer's disease. Genome-wide analyses identified a common variant (rs2997325) influencing cortical PAM that also affected *in vivo* microglial activation measured by positron emission tomography using [^{11}C]-PBR28 in an independent cohort. Finally, we identify overlaps of PAM's genetic architecture with those of Alzheimer's disease, educational attainment, and several other traits.

Background

The function of immune cells in the central nervous system (CNS) has recently become a major focus in human genetics as these cells have been implicated in susceptibility to neurodegenerative, autoimmune, and psychiatric diseases. Microglia, the brain's resident immune cells, are thought to have important roles in both tempering and exacerbating aging-related neuropathological processes; but their precise role remains unclear as they are difficult to access in human subjects. Recently, a molecularly defined subtypes of disease-associated microglia has been proposed to exist in a mouse model of Alzheimer's disease (AD).[1] However, transcriptomic identities of isolated microglia are notoriously plastic[2] and highly susceptible to a myriad of experimental confounders.[3] Regional and temporal heterogeneity of microglia subpopulations has also been shown in human and mouse models based on both molecular and morphological characteristics.

Recent postmortem studies have shown that microglial densities in specific regions are associated with a syndromic diagnosis of both early and late-onset AD,[4] and a recent systematic review of 113 studies quantifying microglial activation in postmortem AD brain highlighted the importance of activation vs. abundance of these cells in disease.[5] However, low sample sizes, indirect measures of microglia, and lack of full antemortem and postmortem pathological assessments all limit the insights that can be drawn from the component studies and this systematic review. Here, we leverage two large unique cohort studies of cognitive aging that include antemortem longitudinal cognitive assessments and structured postmortem histopathological evaluations to characterize a postmortem measure of microglial activation, directly observed by immunohistochemical staining and light microscopy. We first examine how this measure relates to different aging-related pathologies. We follow this with causal mediation

analyses aimed at placing microglial activation temporally within the cascade of pathological events leading to AD. Finally, we perform genome-wide analyses to identify the genomic architecture of microglial activation and deploy a high-resolution polygenic risk scoring method based on Mendelian randomization assumptions to demonstrate putatively causal effects of microglial activation on multiple human diseases and traits.

Methods

Study Subjects

All antemortem cognitive and postmortem data analyzed in this study were gathered as part of the Religious Orders Study and Memory and Aging Project (ROS/MAP),[6–8] two longitudinal cohort studies of elderly, one from across the United States and the other from the greater Chicago area. All subjects were recruited free of dementia (mean age at entry=78±8.7 years), agreed to annual clinical and neurocognitive evaluation, and signed an Anatomical Gift Act allowing for brain autopsy at time of death. *In vivo* [^{11}C]-PBR28 PET imaging acquisitions were collected on data from the Indiana Memory and Aging Study (IMAS), an ongoing neuroimaging and biomarker study based at the Indiana University School of Medicine including elderly subjects at multiple levels of cognitive impairment.[9] Written informed consent was obtained from all ROS/MAP and IMAS participants. Study protocols were approved by each site's Institutional Review Board. Full methods can be found in the appendix.

Genetics, Tanscriptomics, and Proteomics

Genotype array data for 2,067 ROS/MAP subjects was imputed using the Michigan Imputation Server (Haplotype Reference Consortium reference v1.1). For IMAS, data were imputed using IMPUTE v2.2 (1000 Genomes phase 1 reference). *APOE* (rs429358, rs7412) genotyping was carried out separately using standard protocols. RNA sequencing of postmortem dorsolateral prefrontal cortical tissue from 538 subjects were available for analysis at the time of study. Sequencing and standard quality control were performed as previously described.[10] The Speakeasy algorithm[11] was used to cluster expressed genes into functionally-cohesive gene modules, which have been extensively validated for robustness and pathophysiological relevance.[12,13] Average values of gene expression for each of 47 modules were used as

quantitative outcomes. Selected reaction monitoring based (SRM) quantitative proteomics was used to analyze levels of 67 proteins (Supplementary Table 3) in frozen dorsolateral prefrontal cortical tissue from 400 ROS/MAP participants according to a standard protocol.[14,15]

Postmortem Neuropathology, Antemortem Cognitive Decline, and *In Vivo* TSPO PET Imaging

A total of 14 disease- and age-related neuropathologies were measured brain-wide (n=985), as previously published.[16] A subset of up to 225 brain samples were also evaluated for the presence of microglia at three stages of activation in four regions (midfrontal cortex (MF), inferior temporal (IT) cortex, ventral medial caudate (VM), and posterior putamen (PPUT)), based on morphology: stage I (thin ramified processes), stage II (plump cytoplasm and thicker processes), and stage III (appearance of macrophages). A total of 1 932 subjects with genomic data also had longitudinal cognitive performance data available at the time of study. Scans of in vivo [^{11}C]-PBR28 binding were assessed in 27 subjects (n_{CN}=13, n_{MCI}=7, n_{AD} =7) as part of the IMAS study.[9]

Statistical Analysis

Proportion of activated microglia (PAM) scores and association with pathology and cognition

Regression analyses were performed in R (v3.3.3).[17] PAM was calculated by the following formula:

$$PAM_r = \sqrt{\frac{S3_r}{S1_r + S2_r + S3_r}}$$

Where r represents each of four regions and S1, S2, and S3 represent microglial densities measured in region *r* at stage I, II, and III, respectively. To address potential concerns related to PAM distribution and model fitting, we performed extensive model validation and sensitivity

analyses (appendix). Iterative re-weighted least squares robust regression was used and model validation was performed using the .632+ bootstrap method.[18] Models were corrected using the Bonferroni procedure. Causal mediation modeling for identifying direct and indirect effects of PAM on cognitive decline was performed using the 'mediation' R package.

Genome-wide association analysis

GWAS were performed in PLINK[19] (v1.90) using imputed genotype dosages, co-variying for age at death, PMI, sex, genotype batch, and the first three EIGENSTRAT[20] principal components. Significance thresholds of $p<2.5x10^{-8}$ and $p<1.0x10^{-5}$ were deemed genome-wide significant and suggestive, respectfully. Post-processing of GWAS results was conducted using the full complement of state-of-the-art tools available through the recently released Functional Mapping and Annotation of Genome-Wide Association Studies platform (FUMAGWAS; http://fuma.ctglab.nl/).[21]

[^{11}C]-PBR28 PET Imaging Analysis

Statistical Parametric Mapping version 8 (SPM8) was used for imaging analysis. Freesurfer (v5.1) was used to define subject-specific regions of interest and average standardized uptake value (SUV) ratios were extracted and modeled linearly according to rs2997325 genotype.

Polygenic analysis of Summary Statistics

To assess causal relationships between the genetic determinants of cortical PAM (based on our GWAS results) and 29 brain and immune-related traits (and vice versa), we used a genetic risk score-based Mendelian randomization method[22] as implemented in the PRSice[23] program (v1.25). The full list of traits and published GWAS references are listed in Supplementary Table

7. Bonferroni correction was applied for 29 traits in both directions, resulting in a significance threshold of $p < 8.6x10^{-4}$.

Role of the Funding Source

No funding organization or agency played any role in the study design, collection, analysis, and interpretation of data, nor in the writing of the report, nor in the decision to submit for publication. PLDJ had access to all data in the study and final responsibility for the decision to submit for publication.

Data Availability

Access to ROS/MAP data used in the preparation of this manuscript can applied for at the Rush Alzheimer's Disease Center Resource Sharing Hub (https://www.radc.rush.edu/).

Results

Relationship of microglial activation to neuropathologic and cognitive measures

The characteristics of ROS/MAP participants with microglial count data are presented in Table 1. We first performed pairwise spearman correlations of each individual measurement followed by hierarchical clustering (Supplementary Figure 1), finding that stage I microglial densities were more similar between regions, whereas stage II and III microglial densities tended to be more highly correlated within cortical and subcortical regions separately.

Following this observation and prior reports of the presence of morphologically defined active microglia in much smaller samples of AD brains,[5] we performed benchmarking discriminatory analyses for each microglial density phenotype in two stages. First, Welch t-tests comparing mean measures of microglial density between individuals with a postmortem pathological diagnosis of AD vs. non-AD found that total microglial density as measured in any region was not discriminative of AD status ($0.33<p<0.68$; Figure 1a). Expectedly, stage III microglial density was different between AD and non-AD subjects, though this was only true in cortical regions (midfrontal (MF) $p=1.5\text{x}10^{-8}$, Cohen's $d_{[95\%CI]}=0.80[0.52,1.08]$; inferior temporal (IT) $p=6.4\text{x}10^{-9}$, Cohen's $d_{[95\%CI]}=0.84[0.55,1.12]$). Further, a stronger association was observed with the proportion of stage III microglia density relative to total microglia (PAM) (MF $p=1.8\text{x}10^{-10}$, Cohen's $d_{[95\%CI]}=0.91[0.63,1.19]$; IT $p=1.5\text{x}0^{-11}$, Cohen's $d_{[95\%CI]}=0.99[0.70,1.28]$), confirming that morphologically activated microglia rather than the total number of microglia is most important for the accumulation of AD-related pathology in aging[24,25]; this is consistent with earlier work in mice demonstrating that microglial activation rather than proliferation mediates neurodegeneration.[26]

Second, logistic regression modelling of pathological AD in the same sample confirmed our t-test results, finding that models including PAM outperformed other models with a maximum AUC of 0.795 for IT and 0.792 for MF (Figure 1b). Notably, the effects of both cortical PAM measures were independent of and improved model performance to a greater extent than the major *APOE* ε4 genetic risk factor for AD. In the case of IT, the inclusion of PAM increased model performance over the co-variate only model by 18% (AUC=0.745 vs. 0.565), whereas including *APOE* ε4 status only yielded a 9.6% increase (AUC=0.661). Bootstrap analyses reinforced these findings, with calibrated PAM-inclusive models showing 21.4% (IT) and 20.4% (MF) increases in model accuracy vs. the *APOE* ε4 status-inclusive model's 11.9%. In full models containing both *APOE* ε4 status and PAM, the effect sizes of each were comparable for a difference in PAM of one interquartile range (IQR) (MF $OR_{APOE\varepsilon4}$=6.9[2.73,17.4], $OR_{PAMIQR[95\%CI]}$=4.8[2.78,8.15]; IT $OR_{APOE\varepsilon4[95\%CI]}$=6.5[2.39,17.64], $OR_{PAMIQR[95\%CI]}$=4.2[2.46,7.15]). Importantly, neither *APOE* ε4 nor ε2 status were related to either cortical PAM measure, whether or not co-variates were included (all p>0.1).

Having found robust effects of PAM on pathologically defined AD, and given the high degree of neuropathological heterogeneity found in our cohort,[27,28] we sought to identify whether effects of PAM were specific to Aβ and tau (the defining pathologic characteristics of AD) or were also associated with other neuropathological features commonly observed in aged individuals. Using robust regression across 14 pathologies, we found that cortical PAM measures were associated to the greatest extent with total Aβ load and neuritic amyloid plaques, and, to a lesser but still significant extent, with PHF tau, neurofibrillary tangles, and diffuse plaques (Figure 2a). All relationships were in the positive direction, whereby an increase in PAM paralleled an increase in pathology. Notably, we found no significant associations of either subcortical PAM with any

pathology, nor did we find association of any PAM measure with pathologies not related to Aβ or tau accumulation (Figure 2a). Tests of person-specific linear trajectories of cognitive decline revealed significant association of IT PAM with global cognitive decline as well as with decline in all five cognitive sub-domains (Figure 2b). MF PAM was also associated with global cognitive decline, and four of the five cognitive sub-domains. Similar to our neuropathological findings, there were no significant effects of subcortical PAM on cognitive decline.

We next investigated whether activated microglia might contribute to or be the result of accumulating AD pathologies. Mediation analyses found no evidence for direct or mediator effects of PAM on cognitive decline in the presence of PHFtau; rather, these analyses pointed toward indirect effects of cortical PAM on cognitive decline via PHFtau (Supplementary Table 2). Both direct and indirect effects of PAM were found for PHFtau formation, and thus the sum of evidence across our models suggests a synergistic involvement of PAM and Aβ load in affecting global cognitive decline via their effects on PHFtau (Figure 3). Put simply, our data suggest the following chain of events: increased PAM→PHFtau accumulation→worsening cognitive decline. This supports and builds on cross-sectional analyses suggesting that tau correlates best with microglial activation over the course of AD.[29]

Relationship of microglial activation to the cortical transcriptome and protein measures

To further explore the molecular substrates of microglial activation, we accessed whole transcriptome RNA sequencing (RNAseq) and targeted proteomic data from prefrontal cortex and performed robust linear modeling of each PAM measure against expression levels of 47 modules of co-expressed genes (*n*=478 particpants) and 67 proteins of interest (*n*=807).

Proteomic analyses found increases of Aβ peptide to be associated with increased MF (p=1.0x10^{-6}, n=187) and IT PAM (p=2.9x10^{-5}, n=184), providing an independent validation of our observed Aβ-PAM associations from neuropathological assessments (Supplementary Table 3). Levels of VGF were also associated with MF PAM (p=5.3x10^{-4}), whereby lower protein levels were observed with higher PAM. Intriguingly, nominal positive associations (p<0.05) of subcortical PAM were observed for two genes in prefrontal cortex (CIQA and DOCK2) which were recently identified as strongly upregulated in the transcriptome of purified aged human microglia from the same cohort[13] (Supplementary Figure 4a). RNA module expression analyses revealed no significant PAM-module associations after correction, although the pattern of PAM-module associations differed based on region (Supplementary Figure 4b), possibly resulting from the regional specificity of the RNA sequencing data. Thus, PAM does not appear to have a strong effect on the cortical transcriptome, consistent with microglia representing just a small fraction of the total number of cells in cortical tissue.

Genetic architecture of microglial activation

Given the imperfect correlation between MF and IT PAM measures (Spearman ρ=0.66), we performed two separate genome-wide association studies (GWAS). All significant and suggestive GWAS results are listed in Table 2 (details in Supplementary Tables 4 and 5). For IT PAM, a single locus on chromosome 1 reached genome-wide significance (rs183093970; p=5.47x10^{-10}) (Figure 4a,b). However, while the 191kb region encompassed by this lead SNP contains three independent signals, all three have low MAF (0.02>MAF<0.015). Notably, this association was driven by only six individuals in our sample carrying minor alleles tagging this haplotype and should therefore be considered cautiously. Beyond this genome-wide significant

locus, 27 additional independent regions were associated at $p<1x10^{-5}$, and mapping based on position and combined eQTL evidence identified a total of 52 candidate genes (Figure 4c).

For MF PAM, a different locus on chromosome 1 reached genome-wide significance (top SNP: rs2997325^{T} $p=1.88x10^{-8}$, β=0.039, S.E.=0.0066; Figure 4d,e). Beyond this lead SNP, 11 additional regions surpassed our suggestive threshold for association, which mapped to a total of 26 genes (Figure 4f). In contrast to rs183093970, rs2997325 is a relatively common variant (MAF=0.37), lies 8.9 kb 3' of a long intergenic non-coding (Linc) RNA (RP11-170N11.1, LINC01361), and influences the expression of LINC01361 in multiple tissues with combined eQTL mapping evidence of $p=5.35x10^{-12}$.[30] However, *LINC01361* is not measured in our cortical RNAseq data. Q-value analysis revealed no significant overlap in genomic loci implicated by the two PAM GWAS, though many lead SNPs in the MF GWAS did reach nominal significance ($p<0.05$) in the IT GWAS, and vice versa (Supplementary Table 4).

Gene enrichment analyses were performed separately on the two sets of mapped genes. For the 52 genes from the IT PAM GWAS, none of the 30 general tissue types analyzed in GTEx showed Bonferroni significant enrichment (Figure 4j), though in more fine-grained analyses of 53 tissues, sigmoid colon was significantly enriched for differential expression of this gene set (Supplementary Figure 5). Enrichment for functional gene categories and diseases found over 600 significant results, primarily relating to immunologic signatures (Supplementary Table 6A). For the list of 26 mapped genes from the MF PAM GWAS, seven of the 30 general tissue types analyzed in GTEx showed Bonferroni significant enrichment (Figure 4k). In contrast to functional enrichment analyses for the 52 IT PAM GWAS genes, a total of only six unique gene sets showed significant enrichment for MF PAM genes (Supplementary Table 6B). Importantly,

among the 78 genes mapped between both GWAS, eight encoded proteins targeted by known drugs (Supplementary Table 8).

Given the absence of available replication datasets with postmortem microglial staging and genome-wide genotype data, we pursued confirmatory analyses of our GWAS results using another measure of microglial activation: *in vivo* translocator protein (TSPO) positron emission tomography (PET) imaging using the [^{11}C]-PBR28 radioligand. Due to the low MAF of rs183093970, we could only test the genome-wide significant variant from our MF PAM GWAS (rs2997325). In this slightly younger sample (μ_{age}=71.2 years), we found that rs2997325^{T} was significantly associated with an increase in [^{11}C]-PBR28 binding in the entorhinal cortex *in vivo* (p=0.02, r^2=17.1; Figure 4e), consistent with our finding that the same allele increased MF PAM (Figure 4h).

Role of activated microglia across human traits

Having generated genome-wide profiles of genetic risk for both cortical PAM measures, we deployed a high resolution polygenic scoring-based method to test for overlap in the genomic underpinnings of microglial activation and AD, which would suggest a causal link between microglial activation and AD susceptibility. Secondarily, we tested 28 other brain and immune-related traits with publicly available GWAS data to more broadly assess the role of microglia in susceptibility to human disease. For MF PAM (Figure 5a,b), AD showed the strongest polygenic association (p=1.8x10^{-10}, r^2=7.3x10^{-4}), and five other traits had optimal evidence for co-genetic regulation at a corrected threshold, with educational attainment showing the second strongest effect (p=1.1x10^{-5}, r^2=6.2x10^{-5}). For IT PAM, AD susceptibility (p=4.9x10^{-13}, r^2=9.4x10^{-4}) was

also the most strongly associated, and 12 other traits met our significance threshold with educational attainment (p=8.2x10^{-7}, r^2=7.8x10^{-5}) also demonstrating the second strongest effect. These analyses provide evidence that the genetic predisposition to having activated microglia also contributes to making an individual more likely to develop AD. This result therefore goes beyond simply finding an enrichment of AD genes that happen to be expressed in microglia: they provide evidence that genomic propensity for the active microglia state is causally related to AD risk.

The association with educational attainment is intriguing and consistent with our understanding that microglia play an important role in sculpting the developing brain by pruning synapses.[31] Likewise, the association of IT PAM with schizophrenia extends the narrative of the involvement of microglia in this neuropsychiatric disease.[32] To be thorough, we repeated these analyses in the reverse direction, asking whether genetic susceptibility for each of these 29 traits influences microglial activation. In these analyses, we found no association for AD, suggesting that the causal chain of events most likely flows from genetic risk→microglial activation→AD. We did find that primary sclerosing cholangitis (PSC) risk influenced both PAM measures while a few other traits demonstrated single associations (Figure 5c,d). The PSC and inflammatory bowel disease associations may represent shared architecture relating to activated myeloid cells since microglia and peripheral macrophages (which are implicated in these two inflammatory diseases) share many molecular functions.

Discussion

Microglial activation is a well-known phenomenon that has been implicated in a myriad of pathological processes. However, a majority of studies have been conducted either in small numbers of human subjects with limited clinicopathologic data or in murine model systems whose relevance to human disease is unclear given (1) that they do not recapitulate the events and conditions observed in the aging human brain and (2) the emerging understanding of significant differences between aging human and murine microglia.[13,33] Our study provides several important insights. First, microglial activation is not a general feature of the AD brain: we found it to be elevated in cortical but not in subcortical structures. Second, other common neuropathologies of older age do not appear to be significantly associated with activated microglia in the regions tested and therefore do not confound observed associations with Aβ and tau pathologies. Third, our modeling suggests that microglial activation leads to cognitive decline indirectly via the accumulation of PHFtau. This histology-based result is consistent with transcriptome-based findings we have recently reported.[34]

We also describe the previously unmapped genetic landscape of microglial activation measured in postmortem human brain; we found no effect of the *APOE* locus despite reports that APOE may be a ligand for important microglial receptors such as TREM2.[35,36] However, a discovery GWAS returned two significant results: the uncommon rs183093970 variant, whose role remains to be validated, and rs2997325, whose role we confirmed by assessing the related phenotype of *in vivo* microglial PET imaging. The effect of the rs2997325^{T} allele in increasing microglial activation and [^{11}C]-PBR28 binding should be validated more extensively, but, given its high frequency and strong effect, it may be a clinically relevant biomarker requiring attention in the many studies evaluating the utility of other microglia-targeted ligands in a clinical setting to

diagnose or stage neurological diseases. While little is known about the biology of *LINC01362* that appears to be influenced by rs2997325, several of the suggestive loci implicated by our PAM GWAS were found within or near genes of functional significance. For example, the Lymphocyte antigen 75 gene (*LY75*), codes for CD205, a dendritic cell surface receptor that interacts with MHC class I molecules[37] and plays an important role in T cell function.[38] Further investigation of cortical PAM genetic architecture is warranted to extend our initial set of observations.

There are important limitations to consider in our study. First, while we were able to test for some regional-specific effects of PAM on pathology, we did not always have data on pathology in the exact tissue samples in which microglia were counted. Therefore, tightly coupled pathology-microglial associations, such as those known to exist with acute infarction,[39] may have been missed. Whether or not microglial activation is a region-specific phenomenon in aging is an unresolved question; both global and focal distributions have been reported in the aging brain, albeit using different measurements.[40,41] Reassuringly, a recent postmortem investigation of microglial activation measured morphologically in the brains of 11 late onset AD subjects vs. 12 age-matched controls also found increases in microglial activation in cortical but not sub-cortical regions.[4] Second, we have a limited sample size for genome-wide analyses, although it was sufficient to discover the rs2997325 variant which has a strong effect on both microglial activation and *in vivo* imaging. Third, our moderate sample size also means that we cannot exclude that activated microglia may have weak, undetected effects on non-AD pathologies.

Nonetheless, our polygenic analyses revealed significant links that clarify and expand the roles of activated microglia in human diseases. This is clearest for AD where we refine the narrative of the involvement of myeloid cells in AD susceptibility by showing that the proportion of activated

microglia has a causal role in AD. A similar result for cognitive attainment is intriguing as it may be capturing microglia's role in synaptic pruning during development and memory consolidation; however, this is confounded by the fact that this enrichment may also be capturing the role of microglia in age-related cognitive decline that we describe in this report. The enrichment for Crohn's disease is unlikely to represent a causal role of microglia in this disease; rather, this result captures the likely overlap of genetic architecture between activated microglia and other activated myeloid cells in the periphery that are known to be involved in Crohn's disease.

The relevance of recent reports of pathologically important subtypes of microglia in murine model systems, such as disease associated microglia (DAM)[1] and "dark microglia",[42] remains to be demonstrated in the aging human brain since mouse and human microglia diverge significantly in functional molecular signatures with age.[43] By studying activated microglia in the target organ in humans, we have found several key insights, including (1) the observation that they may accelerate cognitive decline through an effect on PHFtau accumulation, which enables us to design mechanistic studies, (2) the discovery and validation of a chromosome 1 locus (among several other suggestive plausible loci) that provides a biological foundation for dissecting the mechanisms of microglial activation, and (3) the strong effect of rs2997325 on [^{11}C]-PBR28 binding which may need to be accounted for in human imaging studies of *in vivo* microglial activation. Thus, microglial activation is a central component of AD susceptibility, and we have begun to elaborate its place in the causal chain of events leading to increased accumulation of tau pathology and subsequent cognitive decline as well as regulatory mechanisms that influence this activation.

Acknowledgements

We would like to thank all of the study participants and acknowledge the essential contributions of Chaya Gopin and Kimberly Cameron to the recruitment and clinical assessments of those participants. We are indebted to the participants in the Religious Orders Study and the Rush Memory and Aging Project. We thank the staff of the Rush Alzheimer's Disease Center. Work was supported by NIH grants P30AG10161, R01AG15819, R01AG17917, R01AG30146, R01NS084965, R01AG048015, U01AG046152, R01LM012535, R03AG054936, the Illinois Department of Public Health, the Translational Genomics Research Institute, and a Postdoctoral Fellowship from the Canadian Institutes of Health Research (CIHR).

Declaration of Competing Interests

The authors have no relevant conflicts of interest to disclose.

Author Contributions

D.F. was responsible for study design, data management and pre-processing, ROS/MAP statistical analyses, and writing of the manuscript. T.R. and E.M.B. contributed to the study design, ROS/MAP statistical analyses, and editing of the final manuscript. S.L.R. and K.N. were responsible for processing IMAS PET imaging data and performing all imaging analyses. V.P. was responsible for the SRM proteomic methodology and analysis, and assisted in editing of the final manuscript. J.A.S. was responsible for overseeing neuropathological data acquisition, ensuring quality control of the data, and editing the final manuscript. A.S. was responsible for IMAS study design and acquisition of IMAS data, and manuscript editing. D.A.B. oversees the ROS/MAP studies, contributed to study design, and assisted in manuscript editing. P.L.D.J.

contributed to the study design, evaluation of results, and writing of the manuscript. All authors read and approved the final manuscript.

References

1. Keren-Shaul, H. *et al.* A Unique Microglia Type Associated with Restricting Development of Alzheimer's Disease. *Cell* **169,** 1276–1290.e17 (2017).
2. Mizee, M. R. *et al.* Isolation of primary microglia from the human post-mortem brain: effects of ante- and post-mortem variables. *Acta Neuropathol. Commun.* **5,** 16 (2017).
3. Gomez-Nicola, D. & Boche, D. Post-mortem analysis of neuroinflammatory changes in human Alzheimer's disease. *Alzheimers Res. Ther.* **7,** 42 (2015).
4. Taipa, R. *et al.* Inflammatory pathology markers (activated microglia and reactive astrocytes) in early and late onset Alzheimer disease: a post-mortem study. *Neuropathol. Appl. Neurobiol.* (2017). doi:10.1111/nan.12445
5. Hopperton, K. E., Mohammad, D., Trépanier, M. O., Giuliano, V. & Bazinet, R. P. Markers of microglia in post-mortem brain samples from patients with Alzheimer's disease: a systematic review. *Mol. Psychiatry* **23,** 177–198 (2018).
6. Bennett, D. A., Schneider, J. A., Arvanitakis, Z. & Wilson, R. S. Overview and findings from the religious orders study. *Curr. Alzheimer Res.* **9,** 628–645 (2012).
7. Bennett, D. A. *et al.* Overview and findings from the rush Memory and Aging Project. *Curr. Alzheimer Res.* **9,** 646–663 (2012).
8. Jager, P. D. *et al.* A multi-omic atlas of the human frontal cortex for aging and Alzheimer's disease research. *bioRxiv* 251967 (2018). doi:10.1101/251967
9. Yoder, K. K. *et al.* Influence of TSPO genotype on 11C-PBR28 standardized uptake values. *J. Nucl. Med. Off. Publ. Soc. Nucl. Med.* **54,** 1320–1322 (2013).
10. Ng, B. *et al.* An xQTL map integrates the genetic architecture of the human brain's transcriptome and epigenome. *Nat. Neurosci.* **20,** 1418 (2017).

11. Gaiteri, C. *et al.* Identifying robust communities and multi-community nodes by combining top-down and bottom-up approaches to clustering. *ArXiv150104709 Phys. Q-Bio* (2015).
12. Mostafavi, S. *et al.* A molecular network of the aging brain implicates INPPL1 and PLXNB1 in Alzheimer's disease. *bioRxiv* 205807 (2017). doi:10.1101/205807
13. Olah, M. *et al.* A transcriptomic atlas of aged human microglia. *Nat. Commun.* **9,** 539 (2018).
14. Petyuk, V. A., Qian, W.-J., Smith, R. D. & Smith, D. J. Mapping Protein Abundance Patterns in the Brain Using Voxelation Combined with Liquid Chromatography and Mass Spectrometry. *Methods San Diego Calif* **50,** 77 (2010).
15. Andreev, V. P. *et al.* Label-free quantitative LC-MS proteomics of Alzheimer's disease and normally aged human brains. *J. Proteome Res.* **11,** 3053–3067 (2012).
16. Bennett, D. A., Wilson, R. S., Boyle, P. A., Buchman, A. S. & Schneider, J. A. Relation of neuropathology to cognition in persons without cognitive impairment. *Ann. Neurol.* **72,** 599–609 (2012).
17. R Core Team. *R: A language and environment for statistical computing*. (R Foundation For Statistical Computing, Vienna, Austria, 2014).
18. Efron, B. & Tibshirani, R. Improvements on Cross-Validation: The .632+ Bootstrap Method. *J. Am. Stat. Assoc.* **92,** 548–560 (1997).
19. Purcell, S. *et al.* PLINK: A Tool Set for Whole-Genome Association and Population-Based Linkage Analyses. *Am. J. Hum. Genet.* **81,** 559–575 (2007).
20. Price, A. L. *et al.* Principal components analysis corrects for stratification in genome-wide association studies. *Nat. Genet.* **38,** 904–909 (2006).

21. Watanabe, K., Taskesen, E., Bochoven, A. & Posthuma, D. Functional mapping and annotation of genetic associations with FUMA. *Nat. Commun.* **8,** 1826 (2017).
22. Johnson, T. Efficient calculation for multi-SNP genetic risk scores. in (2012).
23. Euesden, J., Lewis, C. M. & O'Reilly, P. F. PRSice: Polygenic Risk Score software. *Bioinformatics* **31,** 1466–1468 (2015).
24. Davies, D. S., Ma, J., Jegathees, T. & Goldsbury, C. Microglia show altered morphology and reduced arborization in human brain during aging and Alzheimer's disease. *Brain Pathol. Zurich Switz.* **27,** 795–808 (2017).
25. Serrano-Pozo, A., Gómez-Isla, T., Growdon, J. H., Frosch, M. P. & Hyman, B. T. A Phenotypic Change But Not Proliferation Underlies Glial Responses in Alzheimer Disease. *Am. J. Pathol.* **182,** 2332–2344 (2013).
26. Rogove, A. D., Lu, W. & Tsirka, S. E. Microglial activation and recruitment, but not proliferation, suffice to mediate neurodegeneration. *Cell Death Differ.* **9,** 801–806 (2002).
27. Schneider, J. A., Arvanitakis, Z., Bang, W. & Bennett, D. A. Mixed brain pathologies account for most dementia cases in community-dwelling older persons. *Neurology* **69,** 2197–2204 (2007).
28. Barnes, L. L. *et al.* Mixed pathology is more likely in black than white decedents with Alzheimer dementia. *Neurology* **85,** 528–534 (2015).
29. Serrano-Pozo, A. *et al.* Reactive Glia not only Associates with Plaques but also Parallels Tangles in Alzheimer's Disease. *Am. J. Pathol.* **179,** 1373–1384 (2011).
30. GTEx Consortium *et al.* Genetic effects on gene expression across human tissues. *Nature* **550,** 204–213 (2017).

31. Paolicelli, R. C. *et al.* Synaptic pruning by microglia is necessary for normal brain development. *Science* **333,** 1456–1458 (2011).

32. Notter, T. & Meyer, U. Microglia and schizophrenia: where next? *Molecular Psychiatry* (2017). doi:10.1038/mp.2017.67

33. Ryan, K. J. *et al.* A human microglia-like cellular model for assessing the effects of neurodegenerative disease gene variants. *Sci. Transl. Med.* **9,** (2017).

34. Patrick, E. *et al.* A cortical immune network map identifies a subset of human microglia involved in Tau pathology. *bioRxiv* 234351 (2017). doi:10.1101/234351

35. Yeh, F. L., Wang, Y., Tom, I., Gonzalez, L. C. & Sheng, M. TREM2 Binds to Apolipoproteins, Including APOE and CLU/APOJ, and Thereby Facilitates Uptake of Amyloid-Beta by Microglia. *Neuron* **91,** 328–340 (2016).

36. Krasemann, S. *et al.* The TREM2-APOE Pathway Drives the Transcriptional Phenotype of Dysfunctional Microglia in Neurodegenerative Diseases. *Immunity* **47,** 566–581.e9 (2017).

37. Bonifaz, L. *et al.* Efficient targeting of protein antigen to the dendritic cell receptor DEC-205 in the steady state leads to antigen presentation on major histocompatibility complex class I products and peripheral CD8+ T cell tolerance. *J. Exp. Med.* **196,** 1627–1638 (2002).

38. Fukaya, T. *et al.* Conditional ablation of CD205+ conventional dendritic cells impacts the regulation of T-cell immunity and homeostasis in vivo. *Proc. Natl. Acad. Sci. U. S. A.* **109,** 11288–11293 (2012).

39. Kreisl, W. C. *et al.* Stroke incidentally identified using improved positron emission tomography for microglial activation. *Arch. Neurol.* **66,** 1288–1289 (2009).

40. Simpson, J. E. *et al.* Microglial activation in white matter lesions and nonlesional white matter of ageing brains. *Neuropathol. Appl. Neurobiol.* **33,** 670–683 (2007).

41. Schuitemaker, A. *et al.* Microglial activation in healthy aging. *Neurobiol. Aging* **33,** 1067–1072 (2012).

42. Bisht, K. *et al.* Dark microglia: A new phenotype predominantly associated with pathological states. *Glia* **64,** 826–839 (2016).

43. Galatro, T. F. *et al.* Transcriptomic analysis of purified human cortical microglia reveals age-associated changes. *Nat. Neurosci.* **20,** 1162–1171 (2017).

Figure Legends

Figure 1. **Regional distributions of microglial density phenotypes between pathologically confirmed AD and non-AD subjects and logistic regression model performance**. A) Density plots showing the distributions of all stages of microglia (total count), active microglia (stage III only), and PAM across four autopsied brain regions. *P*-values are two-sided for Welch t-tests of means between AD and non-AD. B) Receiver Operating Characteristic (ROC) curves showing model performance for cortical PAM phenotypes in logistic regression, with pathological AD diagnosis as outcome, and co-variates as specified. Area under the curve (AUC) values are for non-bootstrapped models.

Figure 2. **Robust associations of PAM phenotypes with neuropathology and longitudinal cognitive decline**. A) $-\text{Log}_{10}$(*p*-values), weighted by direction of effect, indicating the strength of evidence for association of each brain-wide neuropathology measure with PAM. B) $-\text{Log}_{10}$(*p*-values), weighted by direction of effect, indicating the strength of evidence for association of each measure of longitudinal cognitive decline with PAM. The red dotted lines on both panels indicate corrected statistical significance thresholds and the blue dotted lines indicate uncorrected $p=0.05$. All *p*-values are two-sided and calculated from parameter estimates of iterative re-weighted least squares regression. Model covariates included age at death, postmortem interval, *APOE* ε4 status, and top three EIGENSTRAT principal components.

Figure 3. **Causal mediation analysis for direct and indirect effects of PAM**. A) illustration of our assumed a priori model of the canonical AD pathological cascade, where beta-amyloid causes tau hyperphosphorylation, which causes downstream cognitive decline. B) Results from eight mediation models, where each black line represents a direct or mediated effect, and the red

X denotes a non-significant effect (p>0.05). C) summary figure showing the proposed causal relationships between phenotypes based on all models tested in panel B.

Figure 4. **Genome-wide association studies (GWAS) of PAM, and TSPO PET imaging follow-up of chromosome 1 locus**. A) Manhattan plot, B) Q-Q plot, and C) locus summary chart for inferior temporal cortex (IT) PAM, and corresponding D) Manhattan plot, E) Q-Q plot, and F) locus summary chart for midfrontal cortex (MF) PAM GWAS. Both analyses co-varied for genotype platform, age at death, sex, postmortem interval, *APOE* ε4 status, and top three EIGENSTRAT principal components. G) Regional association plot highlighting the MF PAM genome-wide significant locus surrounding rs2997325 (p=1.88x10^{-8}). The color of each dot represents degree of linkage disequilibrium at that SNP based on 1000 Genomes Phase 3 reference data. The combined annotation dependent depletion (CADD) score is plotted below the regional association plot on a scale from 0-20, where 20 indicates a variant with highest predicted deleteriousness. The RegulomeDB score is plotted below the CADD score, and summarizes evidence for effects on regulatory elements of each plotted SNP (5 = transcription factor binding site or DNAase peak, 6 = other motif altered, 7 = no evidence). Below the RegulomeDB plot is an eQTL plot showing –log$_{10}$(p-values) for association of each plotted SNP with the expression of the mapped gene RP11-170N11.1 (*LINC01361*). H) Jittered strip chart showing the significant relationship between MF PAM (on y-axis as model residuals after regressing out GWAS co-variates) and rs2997325 genotype. I) Wisker plot showing the means and standard errors of [^{11}C]-PBR28 standard uptake value ratio (SUVR) for the left entorhinal cortex in the PET imaging sample from the Indiana Memory and Aging Study (p = 0.02, r^2=17.1), stratified by rs2997325 genotype. Model co-varied for *TSPO* rs6971 genotype (important biological confounder of [^{11}C]-PBR28 signal), *APOE* ε4 status, age at study entry,

and sex. Finally, tissue enrichment analyses for J) IT and K) MF PAM gene sets in 30 general tissue types from GTEx v7 show Bonferroni significant enrichment (two-sided) of only the MF gene set with colon, salivary gland, breast, small intestine, stomach, lung, and blood vessel tissues. Heat maps showing enrichment for all 53 tissue types in GTEx v7, including uni-directional analyses for up- and down-regulation specifically can be found in Supplementary Figure 5.

Figure 5. **Results of high-resolution polygenic scoring analysis of PAM GWAS and 29 published trait GWAS summary statistics**. A) Stratified violin plots for PAM → published trait polygenic analyses, showing $-\log_{10}$(*p*-values) for genetic score (GRS) associations of inferior temporal cortex (IT) PAM and midfrontal cortex (MF) PAM across all *p*-value thresholds ranging from 0 to 0.5, with 5.0×10^{-5} regular increments (10 000 total scores). Each PAM genetic score was mapped onto the summary statistics of each published GWAS trait and tested for significance. The dotted line represents a corrected statistical significance threshold of $p=8.6 \times 10^{-4}$, corrected for 29 GWAS traits and two PAM measures. The width of each violin represents the density of PAM polygenic scores associated with each trait at a given significance. For example, a bottom-skewed violin (e.g. educational attainment (Edu)) indicates that a majority of scores across the tested set of thresholds tended to achieve greater significance, whereas a top-skewed violin (e.g. bipolar disorder (BPD)) indicates that a majority of tested scores tended toward lower significance. Peaks achieving at least one score above corrected statistical significance are labeled for their respective GWAS trait. B) Network plot illustrating significant results for PAM → GWAS trait analyses, where an arrow indicates a directional effect of a peak PAM GRS on a GWAS trait at corrected significance (edged are labeled with % variance explained in GWAS trait by optimal PAM GRS, and edge thickness is proportional to

the –log(p-value) of the association). C) Stratified violin plots for the GWAS trait → PAM analyses, such that GRS were first calculated across thresholds for published traits and then tested against the PAM summary statistics. D) Network plot illustrating significant results of the GWAS trait → PAM analyses. GRS = genetic risk score; AD = Alzheimer's disease; Edu = educational attainment; IBDCD = irritable bowel disease, Crohn's disease; IBDUC = irritable bowel disease, ulcerative colitis; CAD = coronary artery disease; HIPP = hippocampal volume (from MRI); RA = rheumatoid arthritis; BPD = bipolar disorder; MDD = major depressive disorder; HOMA = homeostasis model assessment (from fasting insulin and glucose); AtopDerm = atopic dermatitis; APOB = circulating Apolipoprotein B; HDL = high density lipoprotein cholesterol; BMDneck = bone marrow density of the neck; SCZ = schizophrenia; ADHD = attention deficit/hyperactivity disorder. The full list of abbreviations found in the legend and descriptions of each published GWAS are listed in Supplementary Table 5.

Tables

Table 1. Summary statistics of ROS/MAP sample included in analysis.

Variable	MF (n=225)	IT (n=219)	VM (n=198)	PPUT (n=218)
Sex (F/M)	147/78	141/78	129/69	140/78
***APOE* ε4 status (-/+)**	178/47	175/44	154/44	172/46
PMI (mean hours, s.d.)	8 (6.9)	8 (6.6)	8 (7.1)	8 (6.9)
Age at study entry (mean years, s.d.)	83 (6)	83 (6)	83 (6)	83 (6)
Age at death (mean years, s.d.)	89 (5.8)	89 (5.8)	89 (5.8)	89 (5.8)
Cognitive AD diagnosis, last visit (CN/MCI/AD)	83/64/71	81/61/71	67/58/67	79/61/71
Postmortem AD diagnosis (AD/non-AD)	90/135	86/133	79/119	86/132

Note: AD = Alzheimer's disease; CN = cognitively normal; F = female; IT = inferior temporal cortex; M = male; MCI = mild cognitive impairment; MF = midfrontal cortex; PMI = postmortem interval; PPUT = posterior putamen.

Table 2. Independent loci identified by cortical PAM GWAS.

Ch	Lead SNP	SNP position	A1	A2	Freq (A1)	Beta (A1)	P-value	Genes mapped to locus (positional and/or eQTL mapping)
Midfrontal cortex PAM								
1	rs2997325	83641424	A	T	0.629	-0.0389	1.88E-08	RP11-170N11.1
1	rs157864	165383761	T	C	0.1415	0.0443	8.60E-06	RXRG
1	rs651691	193958320	T	C	0.5531	0.0317	6.45E-06	
2	rs12623587	232160554	A	C	0.29	-0.0321	6.00E-06	C2orf72, PSMD1, HTR2B, ARMC9
3	rs78461316	104858434	T	C	0.0587	0.0749	2.54E-07	
7	rs141219652	70367062	C	T	0.0226	0.1083	8.72E-06	
10	rs61860520	134826645	T	C	0.0543	-0.0719	4.02E-06	TTC40, LINC01166
11	rs138662357	92058950	C	A	0.0555	0.074	3.49E-07	NDUFB11P1, FAT3, PGAM1P9
13	rs9514523	106927120	T	C	0.1871	-0.0386	9.20E-06	
13	rs9521336	110023731	C	T	0.2146	0.0378	1.96E-06	MYO16-AS1, LINC00399
14	rs2105997	107209226	T	A	0.2276	0.0388	8.46E-06	IGHV4-39, HOMER2P1, IGHV4-61, IGHV3-64, IGHV3-66, IGHV1-69, IGHV3-72, IGHV3-73, IGHV3-74
15	rs144705301	67855035	C	T	0.0263	0.11	1.74E-07	AAGAB, RPS24P16, MAP2K5, SKOR1
Inferior temporal cortex PAM								
1	rs56267558	21005316	T	G	0.1287	0.0431	6.40E-06	MUL1, CDA, PINK1, PINK1-AS, DDOST, KIF17
1	rs113285275	70896319	A	G	0.2344	-0.0328	3.10E-06	HHLA3, CTH
1	rs183093970	88454261	G	A	0.0147	0.1535	5.47E-10	
1	rs147836155	113501607	T	C	0.0129	0.1346	2.46E-06	SLC16A1, SLC16A1-AS1
2	rs148259393	28713654	G	C	0.0204	0.1038	3.30E-06	PLB1
2	rs141418970	40576095	T	G	0.0102	0.1593	4.82E-07	SLC8A1
2	rs17018138	80154236	G	C	0.05	0.0588	7.53E-06	CTNNA2
2	rs79341575	129133292	C	G	0.0551	0.063	2.75E-06	GPR17
2	rs60200364	160708050	A	G	0.0623	0.0555	2.14E-06	BAZ2B, LY75, LY75-CD302, PLA2R1, ITGB6
2	rs2348117	201598521	T	G	0.8893	-0.0414	9.76E-06	AOX3P, AOX2P, AC007163.3, PPIL3, RNU6-312P
3	rs9289581	139405842	T	G	0.37	0.0271	8.32E-06	NMNAT3
4	rs7656795	22398514	T	C	0.8175	-0.037	1.22E-06	GPR125
4	rs114105899	23027094	G	A	0.0158	0.1197	8.10E-07	RP11-412P11.1
4	rs10011717	86136864	A	G	0.3774	-0.0282	6.09E-06	
4	rs77601419	148249054	T	C	0.015	0.1168	2.22E-06	
7	rs77033896	115513816	A	G	0.0169	0.1262	6.84E-07	TFEC, CAV1
8	rs17494322	20673550	G	A	0.075	0.0535	4.18E-06	
11	rs139629925	76144667	G	A	0.0121	0.1347	5.91E-06	RP11-111M22.2, C11orf30, LRRC32
11	rs2084308	111051351	T	A	0.028	0.0967	4.29E-07	
13	rs7328235	41998022	T	C	0.9439	-0.0607	6.72E-06	MTRF1, OR7E36P
13	rs9567982	48605441	G	A	0.1375	0.0394	3.08E-06	LINC00444, LINC00562, SUCLA2, SUCLA2-AS1, NUDT15, MED4, MED4-AS1, POLR2KP2
13	rs117372720	61819169	T	C	0.0149	0.1092	8.97E-06	
13	rs149383020	112585032	A	G	0.0341	0.0787	5.09E-07	
14	rs144434563	91361842	G	A	0.0135	0.1265	6.79E-06	RPS6KA5
14	rs137899216	91830706	T	C	0.0277	0.0911	3.06E-06	GPR68, CCDC88C, SMEK1
17	rs112645358	66248531	T	C	0.0384	0.069	9.94E-06	KPNA2, LRRC37A16P, AMZ2, ARSG
18	rs148222222	65675614	T	C	0.0169	0.1133	1.47E-06	RP11-638L3.1
20	rs71336998	5467150	G	A	0.018	0.1266	1.17E-07	LINC00654

Note: Ch = chromosome; A1 = allele 1 (effect allele); A2 = allele 2; eQTL = expression quantitative trait loci.

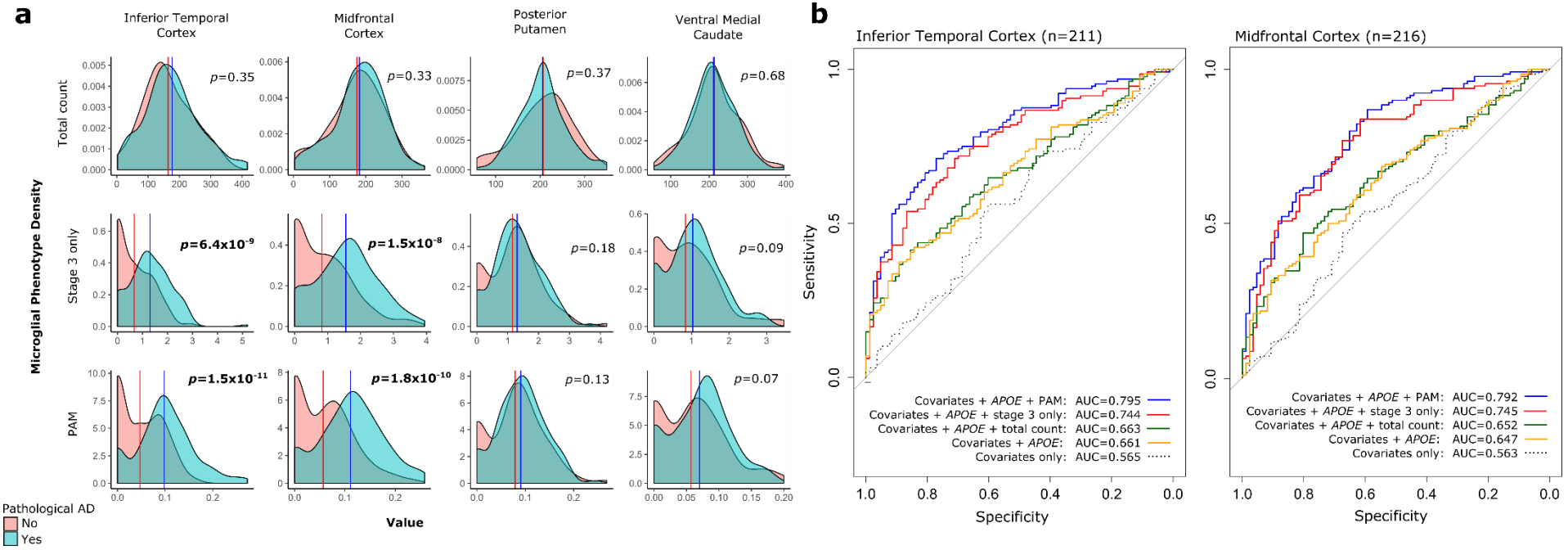
a
Inferior Temporal Cortex
Midfrontal Cortex
Posterior Putamen
Ventral Medial Caudate
Total count
Stage 3 only
PAM
Microglial Phenotype Density
p=0.35
p=0.33
p=0.37
p=0.68
p=6.4x10-9
p=1.5x10-8
p=0.18
p=0.09
p=1.5x10-11
p=1.8x10-10
p=0.13
p=0.07
Value
Pathological AD
No
Yes
b
Inferior Temporal Cortex (n=211)
Midfrontal Cortex (n=216)
Sensitivity
Specificity
Covariates + APOE + PAM: AUC=0.795
Covariates + APOE + stage 3 only: AUC=0.744
Covariates + APOE + total count: AUC=0.663
Covariates + APOE: AUC=0.661
Covariates only: AUC=0.565
Covariates + APOE + PAM: AUC=0.792
Covariates + APOE + stage 3 only: AUC=0.745
Covariates + APOE + total count: AUC=0.652
Covariates + APOE: AUC=0.647
Covariates only: AUC=0.563

Figure 1

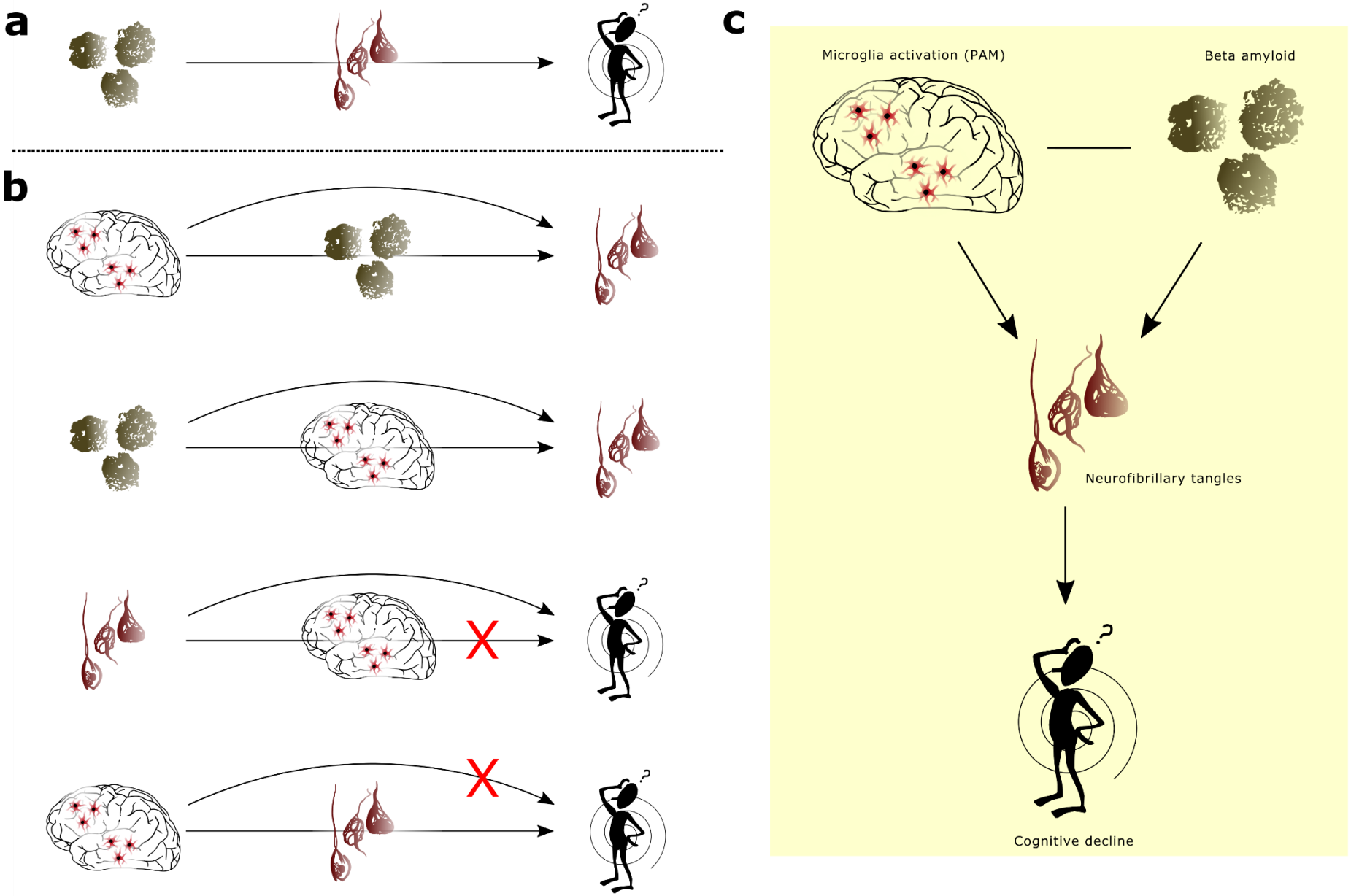
a
b
c
Microglia activation (PAM)
Beta amyloid
Neurofibrillary tangles
Cognitive decline

Figure 2

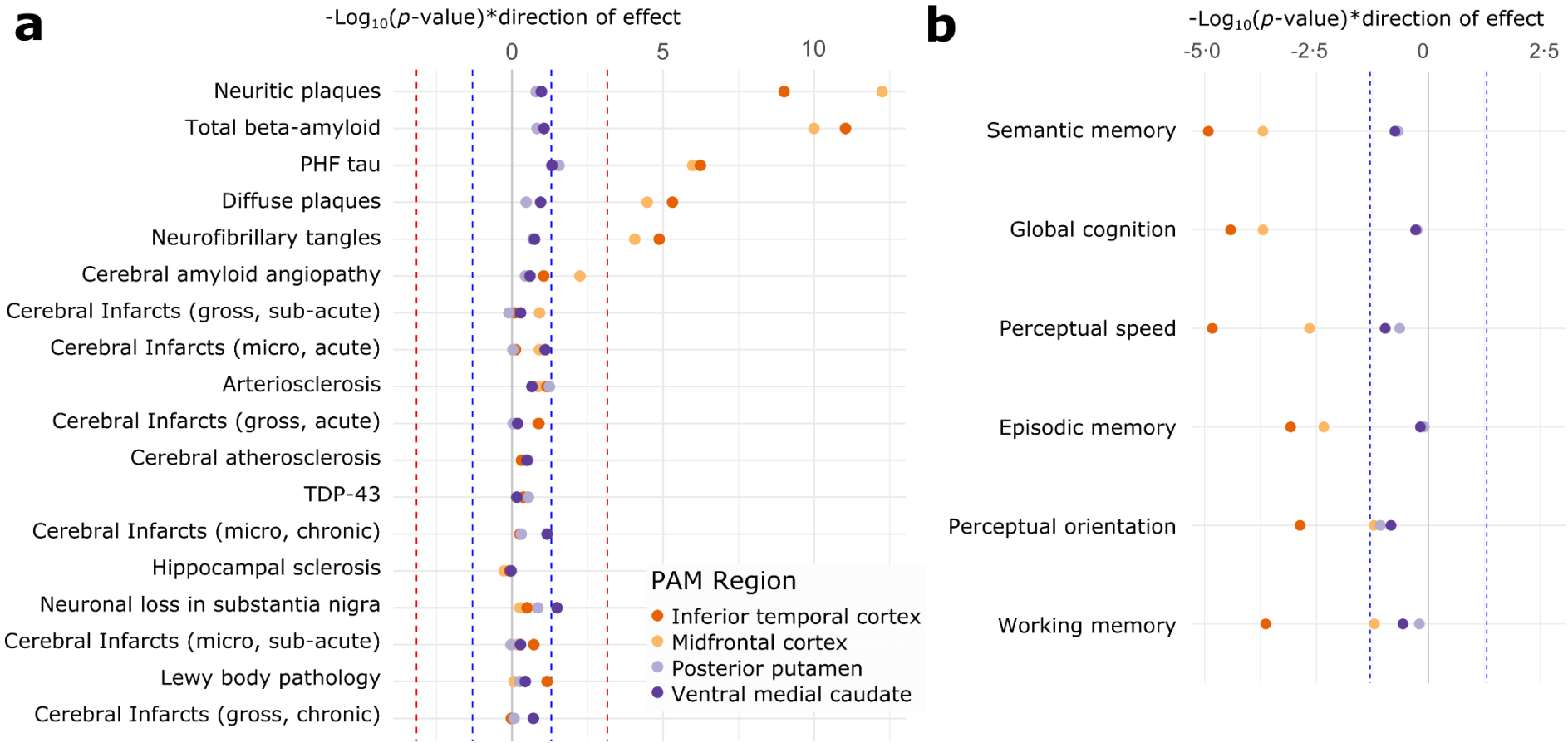
a
-Log10(p-value)*direction of effect
0
5
10
Neuritic plaques
Total beta-amyloid
PHF tau
Diffuse plaques
Neurofibrillary tangles
Cerebral amyloid angiopathy
Cerebral Infarcts (gross, sub-acute)
Cerebral Infarcts (micro, acute)
Arteriosclerosis
Cerebral Infarcts (gross, acute)
Cerebral atherosclerosis
TDP-43
Cerebral Infarcts (micro, chronic)
Hippocampal sclerosis
Neuronal loss in substantia nigra
Cerebral Infarcts (micro, sub-acute)
Lewy body pathology
Cerebral Infarcts (gross, chronic)
PAM Region
Inferior temporal cortex
Midfrontal cortex
Posterior putamen
Ventral medial caudate
b
-Log10(p-value)*direction of effect
-5·0
-2·5
0
2·5
Semantic memory
Global cognition
Perceptual speed
Episodic memory
Perceptual orientation
Working memory

Figure 3

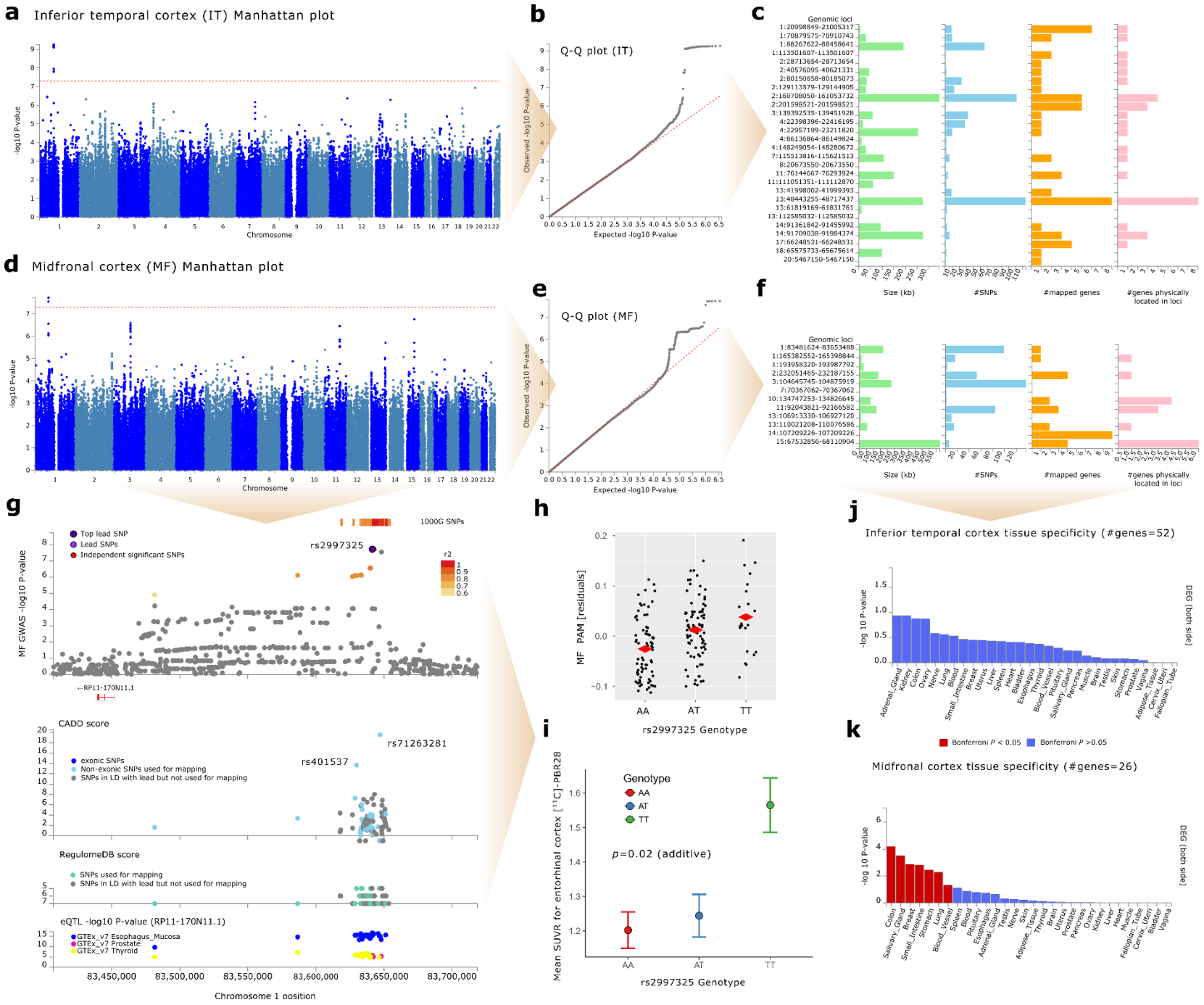
a
Inferior temporal cortex (IT) Manhattan plot
-log10 P-value
Chromosome
b
Q-Q plot (IT)
Observed -log10 P-value
Expected -log10 P-value
c
Genomic loci
Size (kb)
#SNPs
#mapped genes
#genes physically located in loci
d
Midfronal cortex (MF) Manhattan plot
e
Q-Q plot (MF)
f
g
Top lead SNP
Lead SNPs
Independent significant SNPs
1000G SNPs
rs2997325
r2
MF GWAS -log10 P-value
←RP11-170N11.1
CADD score
rs71263281
rs401537
exonic SNPs
Non-exonic SNPs used for mapping
SNPs in LD with lead but not used for mapping
RegulomeDB score
SNPs used for mapping
eQTL -log10 P-value (RP11-170N11.1)
GTEx_v7 Esophagus_Mucosa
GTEx_v7 Prostate
GTEx_v7 Thyroid
Chromosome 1 position
h
MF PAM [residuals]
AA
AT
TT
rs2997325 Genotype
i
Mean SUVR for entorhinal cortex [11C]-PBR28
Genotype
AA
AT
TT
p=0.02 (additive)
rs2997325 Genotype
j
Inferior temporal cortex tissue specificity (#genes=52)
-log 10 P-value
DEG (both side)
k
Bonferroni P < 0.05
Bonferroni P >0.05
Midfronal cortex tissue specificity (#genes=26)

Figure 4

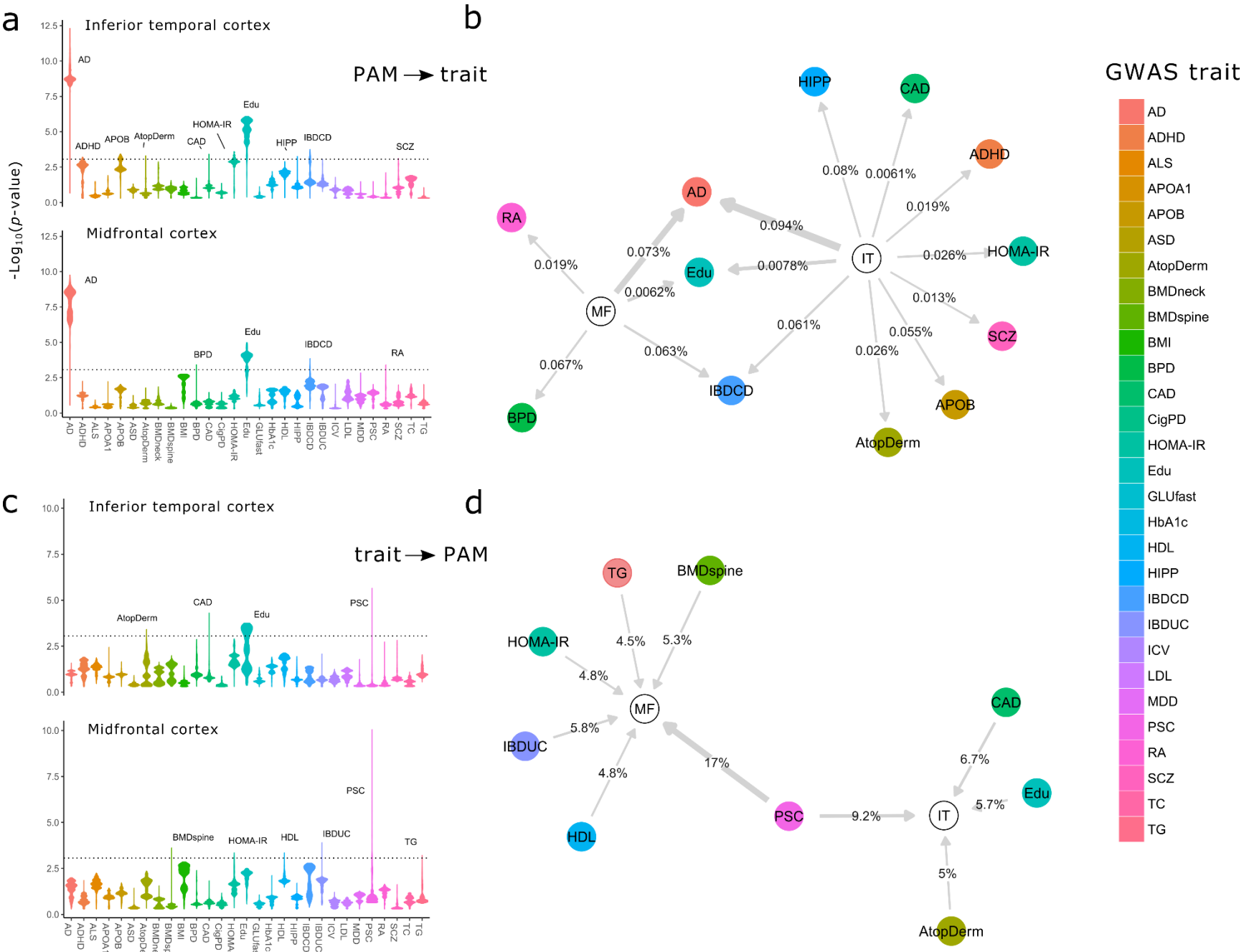
a
Inferior temporal cortex
Midfrontal cortex
-Log10(p-value)
AD
ADHD
APOB
AtopDerm
CAD
HOMA-IR
Edu
HIPP
IBDCD
SCZ
BPD
RA
b
PAM → trait
HIPP
CAD
ADHD
AD
RA
Edu
IT
HOMA-IR
MF
SCZ
IBDCD
APOB
BPD
AtopDerm
0.08%
0.0061%
0.019%
0.094%
0.073%
0.019%
0.0078%
0.026%
0.0062%
0.013%
0.061%
0.055%
0.063%
0.026%
0.067%
GWAS trait
AD
ADHD
ALS
APOA1
APOB
ASD
AtopDerm
BMDneck
BMDspine
BMI
BPD
CAD
CigPD
HOMA-IR
Edu
GLUfast
HbA1c
HDL
HIPP
IBDCD
IBDUC
ICV
LDL
MDD
PSC
RA
SCZ
TC
TG
c
Inferior temporal cortex
Midfrontal cortex
trait → PAM
AtopDerm
CAD
Edu
PSC
BMDspine
HOMA-IR
HDL
IBDUC
TG
d
TG
BMDspine
HOMA-IR
4.5%
5.3%
4.8%
MF
5.8%
IBDUC
CAD
6.7%
4.8%
17%
Edu
5.7%
PSC
9.2%
IT
HDL
5%
AtopDerm

Figure 5